Some Considerations on the Accuracy of the Nonuniform FDTD Method and Its Application to Waveguide Analysis When Combined with the Perfectly Matched Layer Technique

Enrique A. Navarro, Nagula T. Sangary, and John Litva, *Senior Member, IEEE*

***Abstract*— The accuracy of the finite-difference time-domain (FDTD) technique is measured with respect to the mesh's cell dimensions. The accuracy of the FDTD technique is investigated for those applications that demand the use of nonuniform meshes. The results of simulations suggest that second-order accuracy can be achieved. These simulations are carried out using different boundary conditions. It is observed that the choice of boundary conditions plays a large role in the accuracy that is achieved with the FDTD method. The perfectly matched layer (PML) technique is found to be well suited to waveguide analysis because of its wide bandwidth, and the ease with which it can be implemented with a nonuniform mesh. We apply the nonuniform FDTD method, in combination with the PML technique, to analyze a narrow iris in waveguide.**

I. Introduction

INTEREST in the finite-difference time-domain (FDTD) technique has been steadily growing over the past few years [1] because of the technique considerable potential. Numerous problems, which previously were intractable, have been solved using this powerful numerical technique [2], [3]. The FDTD method has been shown to exhibit second-order accuracy in both time and space as long as an uniform mesh is used in both of these dimensions. This conclusion follows directly from the fact that processing is based on centered differences. However, the power of the FDTD method is lost when we try to analyze devices in which small details or sharp edges are involved inside big regions where the field values are soft and vary slowly, then different schemes are needed [4]. In such problems the use of a nonuniform mesh can increase the algorithm's efficiency because a fine mesh can be used in these regions where fine scale structure is present and a coarse mesh in regions where details are absent. References on the use of a nonuniform mesh for dielectric structures can be found in the literature, [5] and [6]. The use of nonuniform meshes has generally been viewed by workers in the field as extending the capabilities of the FDTD technique. However, up to now, no one has discussed the drawbacks of using a nonuniform mesh, such as the errors that are introduced when one uses nonuniform cell sizes.

In general, when partial differential equations are by carrying out numerical analysis on nonuniform grids, the local truncation error at the mesh points will be of first order. Attempts have been made to reduce the magnitude of this error by using grids whose cell sizes vary slowly in the spatial domain. In this case, the sizes of the contiguous cells will change according to $h_i = h_{i-1} + O(h_{i-1}^2)$, with $h_i = h_{i-1}(1 + \alpha \cdot h_{i-1}/L)$ where h_i is the width of cell i in [7] to solve a one-dimensional boundary value problem, $0 < x < L$, and α is a constant. The case $\alpha = 0$ corresponds to a uniform grid. We even entertain expressions for h_i, such as $h_i = h_{i-1}\{1+(\alpha/\pi)[(\pi - x_i)/\pi]^\beta h_{i-1}\}$ where α and β are constants. Depending on the specific problem at hand, there are many choices that can be made for the variation in h_i. Efforts at finding an optimum grid for a determinate boundary value problem can be very time consuming. It follows from the work of Sundqvist [7] that a more complete investigation into the use of grids, having the form $h_i - h_{i-1} = O(h_{i-1}^2)$ would be more than warranted. Kalnay de Rivas [8] carried the work a step further and showed that by varying the size of the grid intervals slowly and monotonically, that is, by using the function $x = x(\psi)$ = smooth function of ψ where $h_i = x(\psi_{i+1}) - x(\psi_i)$, and $\Delta\psi = \psi_{i+1} - \psi_i = constant$, gives approximations of the first and second derivatives with second-order accuracy, since the truncation errors due to the nonuniformity of the grid are of second-order in $\Delta\psi$. Subsequently it was pointed out that a convenient choice is $x = P_n(\psi)$, where P_n is a polynomial. In particular, the simplest choice is $x = \psi^2$.

The work of Manteuffel and White on the numerical solutions of scalar boundary value problems, using nonuniform meshes [9], shows that for many common difference schemes, the accuracy is second-order in spite of the first-order truncation error, and with no restrictions on the characteristics of the nonuniform grid. However, it was pointed out that the accuracy in cell centered difference schemes is influenced by the boundary conditions, particularly the form of the truncation error resulting from the boundary conditions, and the values of the constants involved. In a recent work [10], Monk and Suli proved that the FDTD scheme is also second-order convergent regardless of the mesh nonuniformity. The demonstration of

Manuscript received November 10, 1995; revised March 20, 1996.

E. A. Navarro is with the Department of Applied Physics, Universitat de València, Doctor Moliner 50, 46100 Burjassot, València, Spain.

N. T. Sangary and J. Litva are with the Communications Research Laboratory, McMaster University, Hamilton, Ont., L8S 4K1, Canada.

Publisher Item Identifier S 0018-9480(96)04715-1.

the second-order properties was based on a previous work on finite volume approximations for the Poisson equation [11] and had the fact that Yee's scheme is also a finite volume scheme. The proof also used the assumption of Dirichlet homogeneous boundary conditions.

In this paper, we carry out a numerical investigation of the accuracy of the nonuniform FDTD method and present the results. The results obtained from the FDTD simulations are compared with analytical values for different boundary conditions. Using the results of the computer simulations it will be shown that the use of nonuniform grids with FDTD yields numerical values of the fields that have second-order accuracy with respect to the cell dimensions. This accuracy is achieved when the FDTD method is used in combination with "perfect" Boundary Conditions. When "nonperfect" boundary conditions are used, the accuracy degrades to first order. In the presented analysis we consider: homogeneous Dirichlet boundary condition, the perfectly dispersive boundary condition for waveguides [12], and the perfectly matched layer (PML) [13]–[15]. The PML's are adapted to the nonuniform mesh and are found more convenient than second-order dispersive boundary conditions. Finally we show the application of the nonuniform FDTD in combination with PML for analyzing narrow iris-discontinuities in waveguide. Although one might approach the narrow iris problem by combining the FDTD method with the Bethe's small hole theory, [16], the time domain results are wanting in terms of accuracy, which in turn leads to greater errors after applying the Fourier transform. Our FDTD results are compared with mode matching results and measurements and are observed to be in close agreement.

II. Theory

A. The FDTD Method in Nonuniform Grids

The nonuniform FDTD algorithm for an isotropic medium can be easily derived from the integral form of Maxwell's equations [17]. However, the derivation follows directly from Yee's original scheme. For a nonuniform mesh, as shown in Fig. 1, where the electric field components are located along the edges of the cells, and the magnetic field components are located on the faces of the cells, the discretized form of the equation for the E_x field component is

$$\epsilon \frac{E_x^{n+1} - E_x^n}{\Delta t} \cdot S|_{(i,j,k)} = H_z^{n+1/2}(i, j+1/2, k) \cdot \Delta z(i, j+1/2, k) - H_z^{n+1/2}(i, j-1/2, k) \cdot \Delta z(i, j-1/2, k) - H_y^{n+1/2}(i, j, k+1/2) \cdot \Delta y(i, j. k+1/2) + H_y^{n+1/2}(i, j, k-1/2) \cdot \Delta y(i, j, k-1/2) \quad (1)$$

where S is the surface enclosed by the path of integration. Since the mesh is orthogonal, $\Delta z(i, j-1/2, k) = \Delta z(i, j+1/2, k) = \Delta z(k)$, $\Delta y(i, j, k-1/2) = \Delta y(i, j, k+1/2) = \Delta y(j)$, and $S|_{(i,j,k)} = \Delta z(k) \cdot \Delta y(j)$. Therefore, we can write

$$E_x^{n+1}(i, j, k) = E_x^n(i, j, k) + \frac{\Delta t}{\epsilon} \cdot \left[\frac{H_z(i, j+1/2, k) - H_z(i, j-1/2, k)}{\Delta y(j)} - \frac{H_y(i, j, k+1/2) - H_y(i, j, k-1/2)}{\Delta z(k)} \right]^{n+1/2} \quad (2)$$

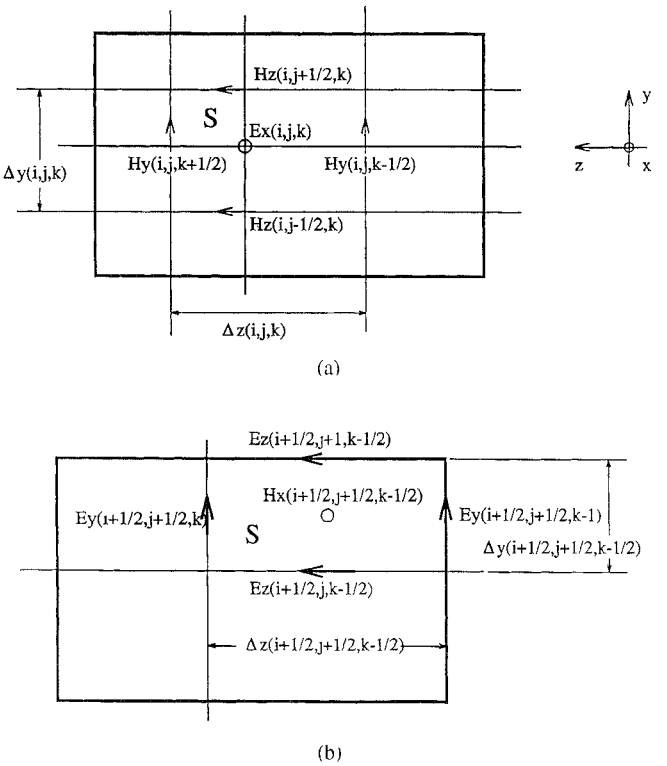

Fig. 1. Nonuniform FDTD cell

The equations for E_y, E_z, H_x, H_y, and H_z are derived similarly.

For each field location, the cell dimensions $\Delta x(i)$, $\Delta y(j)$, and $\Delta z(k)$ are stored in computer memory. $\Delta x(i)$, $\Delta y(j)$, and $\Delta z(k)$ are one-dimensional arrays whose storage requirement is small in comparison with the three-dimensional arrays of the field components.

B. The Perfect Dispersive Boundary Condition

In a rectangular waveguide the dominant mode is the TE_{10}, and this can be explained as a combination of two plane waves travelling with angle γ with respect to the conducting walls. This angle is related to the frequency, and the dimensions of the waveguide, therefore a first-order perfectly dispersive boundary condition can be developed to absorb the propagating monochromatic wave [12], [18]. The combination of two first-order DBC's gives a second-order one that exactly absorbs two monochromatic waves [12]. This absorbing boundary condition is similar to the Litva's boundary condition that is used in the FDTD analysis of microstrip circuits [19]. The first-order perfect dispersive boundary condition in a waveguide is applied to the tangential field components and can be written as

$$\sqrt{1 - \left(\frac{1}{2af}\right)^2} \frac{\partial U}{\partial t} - \frac{1}{\sqrt{\mu\epsilon}} \frac{\partial U}{\partial x} = 0 \quad (3)$$

where U is either E_y, or E_z, when is applied at the y–z-plane, a is the waveguide width and f is the frequency.

C. The Perfectly Matched Layer

We present a formulation of the PML that can be interfaced with the nonuniform FDTD scheme. To implement the PML, we split each field component E_i into two subcomponents, E_{i-j} and E_{i-k}, so that the discretization of Maxwell's curl equations in the PML region become

$$E_{xy}(i,j,k)^{n+1} = Ae_y(j) \times E_{xy}(i,j,k)^n - Be_y(j) \cdot \left[\frac{H_z(i,j+1/2,k) - H_z(i,j-1/2,k)}{\Delta y(i)}\right]^{n+1/2} \quad (4)$$

$$E_{xz}(i,j,k)^{n+1} = Ae_z(k) \times E_{xz}(i,j,k)^n - Be_z(k) \cdot \left[\frac{H_y(i,j,k-1/2) - H_y(i,j,k+1/2)}{\Delta z(k)}\right]^{n+1/2} \quad (5)$$

$$E_{yx}(i,j,k)^{n+1} = Ae_x(i) \times E_{yx}(i,j,k)^n - Be_x(i) \cdot \left[\frac{H_z(i-1/2,j,k) - H_z(i+1/2,j,k)}{\Delta x(i)}\right]^{n+1/2} \quad (6)$$

$$E_{yz}(i,j,k)^{n+1} = Ae_z(k) \times E_{yz}(i,j,k)^n - Be_z(k) \cdot \left[\frac{H_x(i,j,k+1/2) - H_x(i,j,k-1/2)}{\Delta z(k)}\right]^{n+1/2} \quad (7)$$

$$E_{zx}(i,j,k)^{n+1} = Ae_x(i) \times E_{zx}(i,j,k)^n - Be_x(i) \cdot \left[\frac{H_y(i+1/2,j,k) - H_y(i-1/2,j,k)}{\Delta x(i)}\right]^{n+1/2} \quad (8)$$

$$E_{zy}(i,j,k)^{n+1} = Ae_y(j) \times E_{zy}(i,j,k)^n - Be_y(j) \cdot \left[\frac{-H_x(i,j+1/2,k) + H_x(i,j-1/2,k)}{\Delta y(j)}\right]^{n+1/2} \quad (9)$$

and for the magnetic field components

$$H_{xy}(i,j,k)^{n+1/2} = Ah_y(j) \times H_{xy}(i,j,k)^{n-1/2} - Bh_y(j) \cdot \left[\frac{E_z(i,j+1/2,k) - E_z(i,j-1/2,k)}{\Delta y(j)}\right]^{n} \quad (10)$$

$$H_{xz}(i,j,k)^{n+1/2} = Ah_z(k) \times H_{xz}(i,j,k)^{n-1/2} - Bh_z(k) \cdot \left[\frac{-E_y(i,j,k+1/2) + E_y(i,j,k-1/2)}{\Delta z(k)}\right]^{n} \quad (11)$$

$$H_{yx}(i,j,k)^{n+1/2} = Ah_x(i) \times H_{yx}(i,j,k)^{n-1/2} - Bh_x(i) \cdot \left[\frac{E_x(i,j,k+1/2) - E_x(i,j,k-1/2)}{\Delta z(k)}\right]^{n} \quad (12)$$

$$H_{yz}(i,j,k)^{n+1/2} = Ah_z(k) \times H_{yz}(i,j,k)^{n-1/2} - Bh_z(k) \cdot \left[\frac{-E_z(i+1/2,j,k) + E_z(i-1/2,j,k)}{\Delta x(i)}\right]^{n} \quad (13)$$

$$H_{zx}(i,j,k)^{n+1/2} = Ah_x(i) \times H_{zx}(i,j,k)^{n-1/2} - Bh_x(i) \cdot \left[\frac{E_y(i+1/2,j,k) - E_y(i-1/2,j,k)}{\Delta x(i)}\right]^{n} \quad (14)$$

$$H_{zy}(i,j,k)^{n+1/2} = Ah_y(j) \times H_{zx}(i,j,k)^{n-1/2} - Bh_y(j) \cdot \left[\frac{-E_x(i,j+1/2,k) + E_x(i,j-1/2,k)}{\Delta y(j)}\right]^{n} \quad (15)$$

where $E_x = E_{xy} + E_{xz}$, $E_y = E_{yx} + E_{yz}$, $E_z = E_{zx} + E_{zy}$, and $H_x = H_{xy} + H_{xz}$, $H_y = H_{yx} + H_{yz}$, $H_z = H_{zx} + H_{zy}$.

For the conventional FDTD integration the coefficients $Ae - h_i(l)$, $Be - h_i(l)$ are

$$Ah_i(l) = \frac{1 - \frac{\sigma_i^*(l)\Delta t}{2\mu}}{1 + \frac{\sigma_i^*(l)\Delta t}{2\mu}} \quad (16)$$

$$Bh_i(l) = \frac{\Delta t}{\mu\left[1 + \frac{\sigma_i^*(l)\Delta t}{2\mu}\right]} \quad (17)$$

$$Ae_i(l) = \frac{1 - \frac{\sigma_i(l)\Delta t}{2\epsilon}}{1 + \frac{\sigma_i(l)\Delta t}{2\epsilon}}, \quad (18)$$

$$Be_i(l) = \frac{\Delta t}{\epsilon\left[1 + \frac{\sigma_i(l)\Delta t}{2\epsilon}\right]}. \quad (19)$$

If the condition $\sigma_i/\epsilon_o = \sigma_i^*/\mu$ is enforced, the field components inside the PML region suffer a strong attenuation in the i-direction. The decay is so rapid that the conventional time integration of the FDTD method is not useful; instead, an exponential time integration is performed in the PML region, [20]. For the exponential time integration inside the PML region, the coefficients are

$$Ah_i(l) = \exp\left[-\frac{\sigma_i^*(l)\Delta t}{\mu}\right] \quad (20)$$

$$Bh_i(l) = \frac{\exp\left[-\frac{\sigma_i^*(l)\Delta t}{\mu}\right] - 1}{\sigma_i^*(l)} \quad (21)$$

$$Ae_i(l) = \exp\left[-\frac{\sigma_i(l)\Delta t}{\epsilon}\right], \quad (22)$$

$$Be_i(l) = \frac{\exp\left[-\frac{\sigma_i^*(l)\Delta t}{\epsilon}\right] - 1}{\sigma_i(l)}. \quad (23)$$

In theory a single absorbing layer would be enough, but in practical FDTD applications, the discretization of the PML region into several layers has been proved to be more convenient. In this way, we introduce $(\sigma_x^*, \sigma_x, 0, 0, 0, 0)$ for the walls defined by x = constant, $(0, 0, \sigma_y^*, \sigma_y, 0, 0)$ for those with y

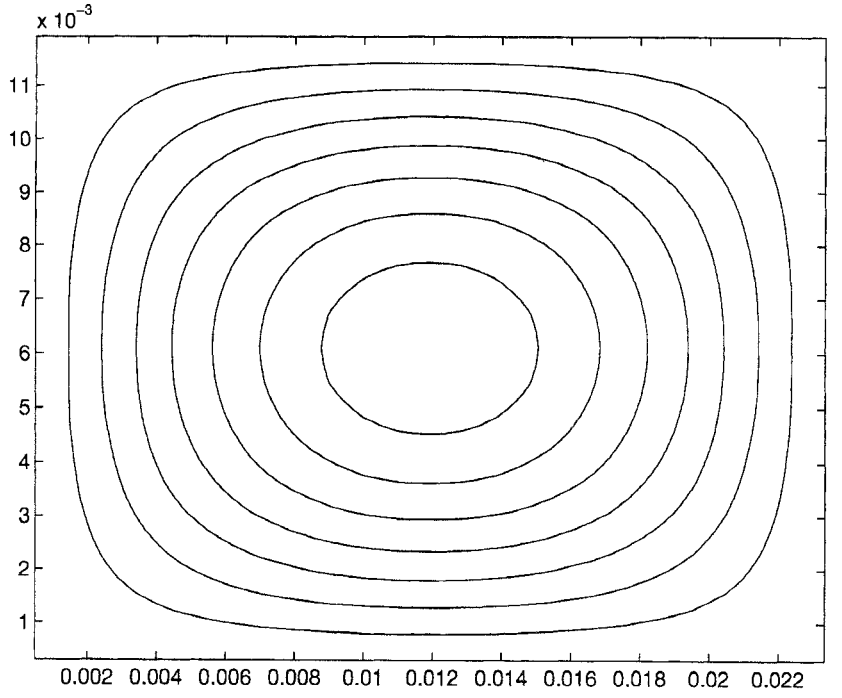

Fig. 2. Contour lines E_z = constant for the TM_{11} mode, waveguide cross section 2.286 × 1.16 cm^2, regular mesh 50 cells in x, 40 cells in y-dimension.

= constant, $(\sigma_x^*, \sigma_x, \sigma_y^*, \sigma_y, 0, 0)$ along the intersection of the x–y walls and $(\sigma_x^*, \sigma_x, \sigma_y^*, \sigma_y, \sigma_z^*, \sigma_z)$, for the intersection of the x–y–z walls. In the waveguide analysis with nonuniform FDTD, the number of layers used in each PML region and the profile of the conductivity will depend on the cell size, [13]. In practical applications ten cells are enough in which the conductivity is gradually increased in the penetrating direction, orthogonal to each PML region. For instance, the PML region at the planes i = constant will have an increased conductivity in the i direction given by $\sigma_i(d) = \sigma_{i_{\max}}(d/D)^2$, where D is the total width of the PML region, and d is the penetration distance inside the PML region. $\sigma_{i_{\max}}$ is adjusted at each PML wall in order to get an apparent reflection coefficient given by,

$$R = \exp -2\sigma_{i_{\max}} D\sqrt{\frac{\mu}{\epsilon}}. \tag{24}$$

III. Numerical Analysis of the FDTD Error

Throughout this section, we will be interested in determining the error that is introduced into the FDTD method by using a nonuniform mesh. As long as we are mindful of the requirements for carrying out full spatial discretization, we avoid the need to consider the dispersion that can be found in [21]. In the present section, we will be considering the magnitudes of fields in either a two-dimensional resonator (cross-section of a waveguide) or the propagation in a matched waveguide.

A. Error Analysis with Homogeneous Dirichlet Boundary Conditions

The FDTD method is used to obtain the TM_{11} mode in a rectangular waveguide following the procedure given by Navarro *et al* in [22]. The TM_{11} field distribution is analytically known in a waveguide, thus the difference between the field obtained numerically and that obtained analytically will give us an estimation of the numerical error of the FDTD method when it is applied to a nonuniform mesh. The electromagnetic field is introduced in the x–y transversal section of the waveguide, by using a time domain pulse, consisting solely of an E_z-component. The time domain pulse resonates within the two-dimensional slice of the waveguide and the first resonant field corresponds to the TM_{11} mode [22]. The field corresponding to the TM_{11} mode is extracted from the time domain fields by applying the discrete Fourier transform to the time domain fields at each mesh point. The

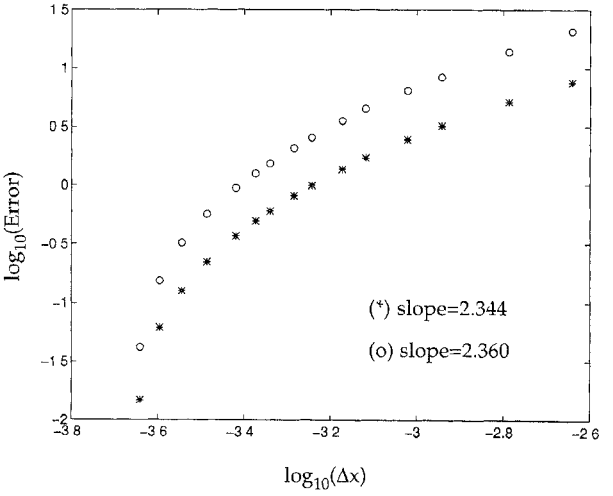

Fig. 3. Decimal logarithm of the numerical error in calculating TM_{11} mode using an uniform mesh against decimal logarithm of the cell dimension. Inset: slope for a least square adjust. (o) Error = maximum Error, $\Delta x = \Delta x_{\text{maximum}}$. (*) Error = average Error, $\Delta x = \Delta x_{average}$.

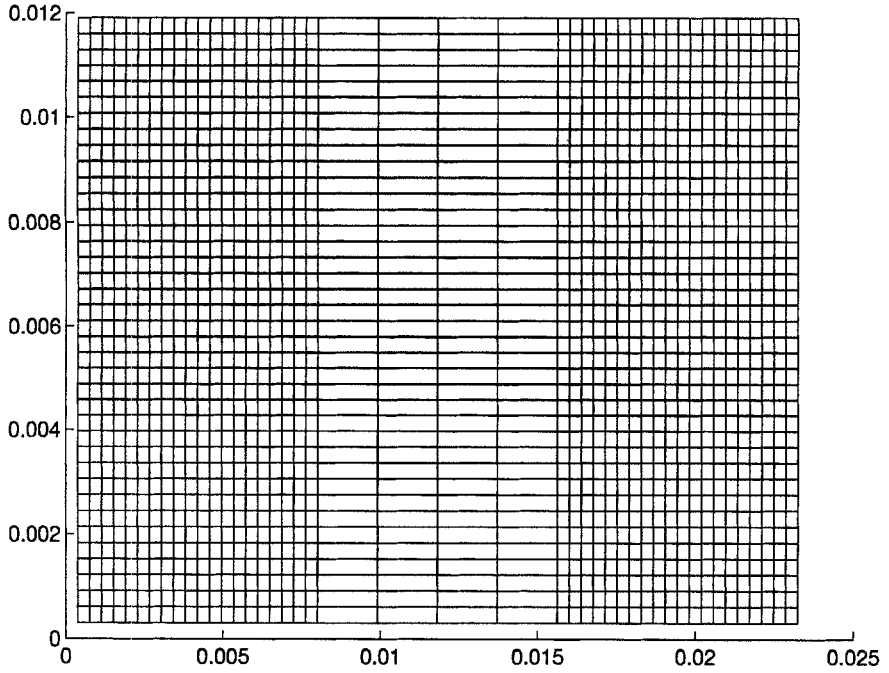

Fig. 4. Nonuniform mesh for the cross section of the waveguide with abrupt change in cell dimensions.

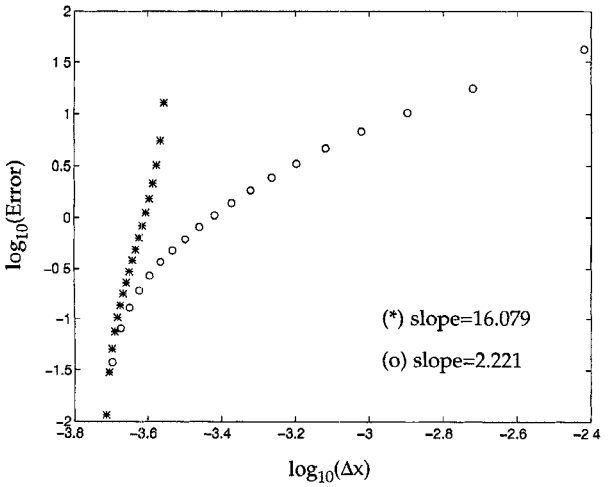

Fig. 5. Numerical error in calculating TM_{11} mode using a nonuniform mesh with abrupt change in cell dimensions. Inset: slope for a least square adjust. (o) Error = maximum Error, $\Delta x = \Delta x_{\text{maximum}}$. (*) Error = average Error, $\Delta x = \Delta x_{average}$.

TM_{11} mode is compared with analytical values to evaluate the errors generated at the nodes of: a) a set of uniform meshes, b) a nonuniform mesh with abrupt changes in the dimension of its cells, and c) gradually changing nonuniform meshes. In every case the dimensions of the mesh in y-direction is kept constant in order to keep the error due to the discretization in the y-direction a constant. The cross section of the waveguide has dimensions 2.286 × 1.16 cm^2.

To start, we show the numerical error that is generated when one uses an uniform mesh. The lines of E_z = constant, obtained with a 50 × 40 grid, are plotted in Fig. 2. The maximum error is calculated as the maximum of the absolute value of the difference between the theoretical field and the numerically simulated field in the nodes. The average error is obtained averaging for every field node the absolute value of the difference between the theoretical and the numerical field. In Fig. 3 are presented both the maximum error versus cell size, and the average error versus cell size (decimal logarithm), these points are adjusted to a straight line with a least squares algorithm. In both cases, the results confirm, the theoretical predicted second-order accuracy. The maximum error has a slope of 2.360 and the slope for the average error is 2.344. The average error is calculated by adding the absolute value of the errors at each node and dividing by the number of nodes.

In Fig. 4 is shown an example of the nonuniform meshes that are used for the analysis of the waveguide problem. Uniform meshes are used on the left and right sides of the structure. A coarse mesh is used in its middle. The cell ratio between contiguous regions was as small as 1.0526 and large as 20. The maximum error versus maximum cell dimension and the average error versus average cell dimension are plotted in Fig. 5. For the first case, we obtain a slope of 2.221, and for the average error we get a slope of 16.079.

In Fig. 6 is presented a gradually changing nonuniform mesh. The ratio of change between adjacent cells varies between 1.1–2.5. In Fig. 7 the errors attributed to the nonuniform mesh are plotted versus cell dimensions, and the slope of the best fit for maximum errors is 1.917 and is 2.376 for the average errors. Although some discussion is warranted with regards the difference in the trends of these errors, depending on the type of mesh, the error is of second-order, or more, with the cell dimension.

B. Error Analysis with the Perfect Dispersive Boundary Condition

The perfectly dispersive boundary condition in waveguides [12], is a first-order absorbing boundary condition that can be

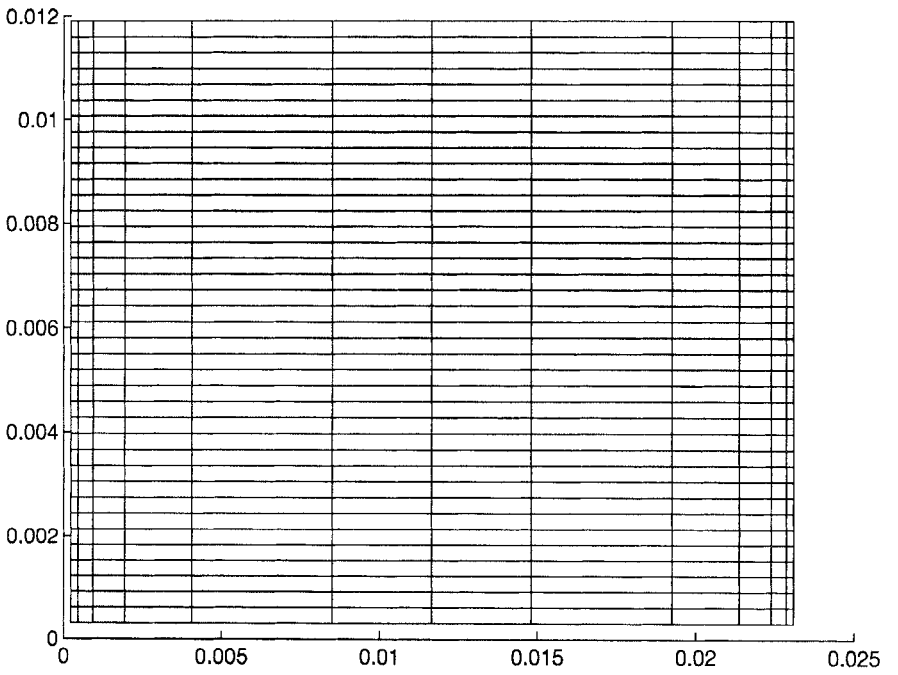

Fig. 6 Example of a gradual nonuniform mesh.

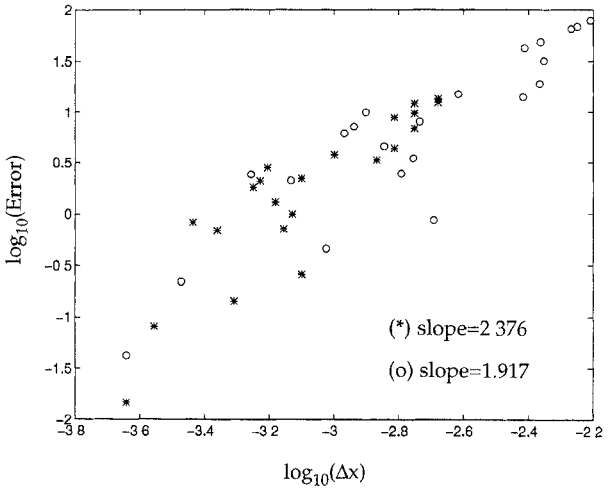

Fig. 7. Numerical error in calculating TM_{11} mode using a gradual nonuniform mesh. Inset: slope for a least square adjust. (o) Error = maximum Error, $\Delta x = \Delta x_{\text{maximum}}$. (*) Error = average Error, $\Delta x = \Delta x_{average}$.

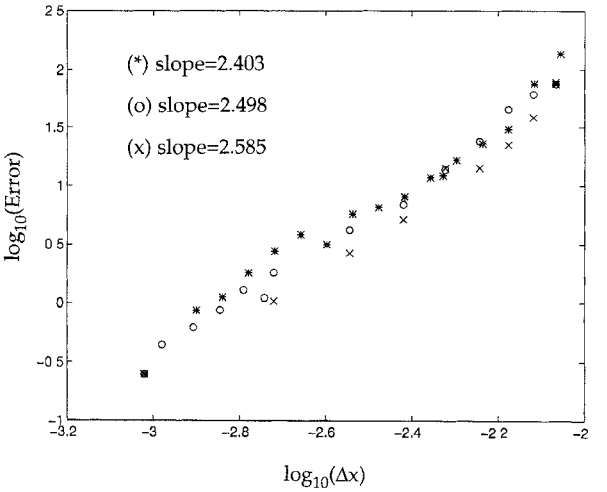

Fig 8. Maximum error versus maximum cell size using the perfect dispersive boundary condition: (×) Uniform mesh. (o) Nonuniform with abrupt change. (*) Gradual nonuniform.

adjusted to give near ideal results at a particular frequency for a propagating field. The reason being that the wave velocity is known, which allows us to build a highly accurate numerical absorbing boundary condition. In other words, since the angle of incidence of the plane waves with the boundary are known [12], we are able to develop highly accurate boundary conditions. We will use simulations for a waveguide, subjected to a monochromatic source of TE_{10} fields, and a perfect DBC located at the far end of the waveguide. A large number of different grids are used, namely:

1) uniform grids with different cell dimensions;
2) nonuniform grids in the axis of the propagating direction:
   a) Two uniform regions connected with change in spatial increment ranging from 1 : 1 to 1 : 9.
   b) A nonuniform mesh in which the dimension of the cell increases gradually. In this case we adopt an exponentially increase of the form $h_{i+1} = h_i \times s$ where s is the growth factor between two adjacent cells, and the ratio $h_{\max}/h_{\min}$ varied between 1 : 1 and 1 : 9 roughly. In both a) and b) we use the same monochromatic source for the pure TE_{10} field, as well as the same DBC used previously. In cell instances the perfect dispersive boundary condition is applied to the last cell i.e., the cell marking the edge of the mesh. The discrete Fourier transform is performed at every electric field node point located in the waveguide. In that way the maximum error and average error are calculated as

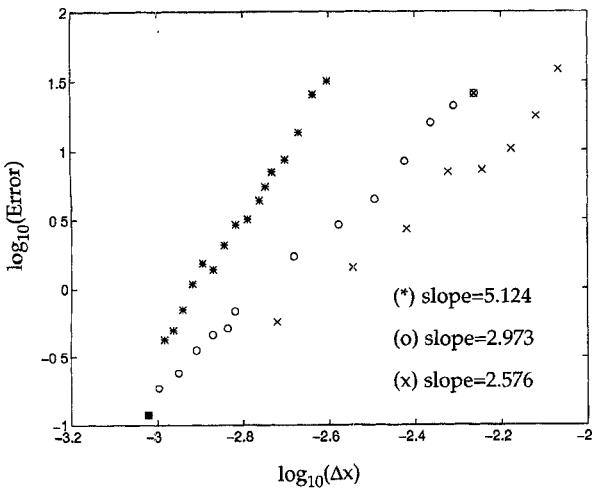

Fig. 9. Average error versus average cell size using the perfect dispersive boundary condition: (×) Uniform mesh. (o) Nonuniform with abrupt change. (*) Gradual nonuniform.

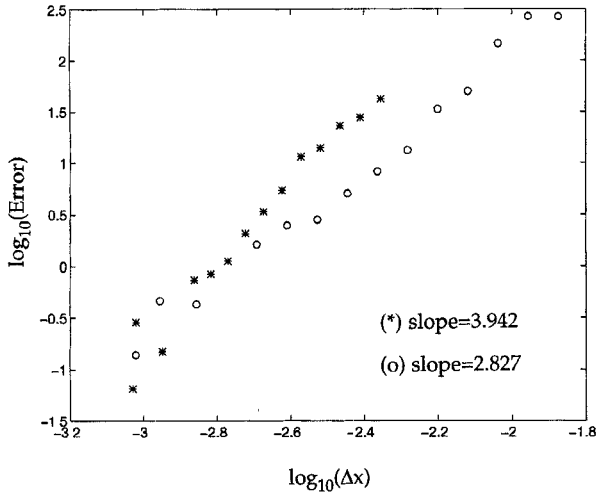

Fig. 10. Error versus cell size using the Perfect Matched Layer in a combined gradual and abrupt changed mesh: (o) Error = maximum Error, $\Delta x = \Delta x_{\text{maximum}}$. (*) Error = average Error, $\Delta x = \Delta x_{average}$.

the difference between the numerically obtained data and the theoretically obtained from the excitation value of the TE_{10} source. In Fig. 8 is plotted the maximum error versus spatial increment for case 1), 2a), and 2b), and in Fig. 9 is plotted the average error versus average cell dimension. The least squares fit of the decimal logarithm of the error results versus the decimal logarithm of the cell dimension is calculated in each case and showed in the inset of Figs. 8 and 9. These results are illuminating and give a good insight into the errors that occur when the FDTD method is used with a proper absorbing boundary condition. The results show that in spite of the mesh being nonuniform, second-order accuracy is achieved with the FDTD method for the maximum error. This conclusion remains true for meshes with many different types of nonuniformity. The average error is observed to be dependent on

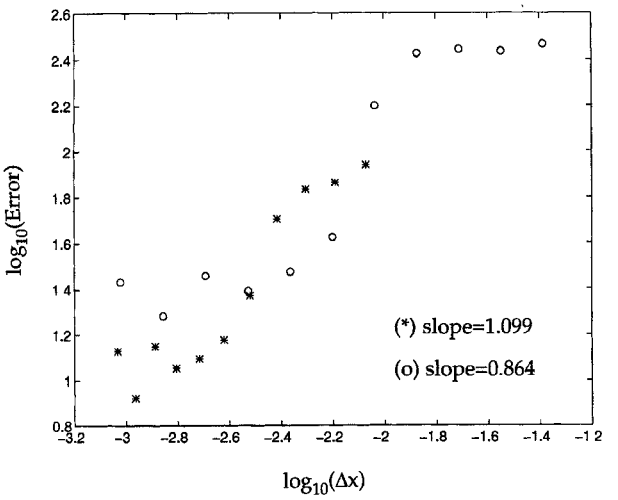

Fig. 11. Error versus cell size using an "imperfect" first-order absorbing boundary in a combined gradual and abrupt changed mesh: (o) Error = maximum Error, $\Delta x = \Delta x_{\text{maximum}}$. (*) Error = average Error, $\Delta x = \Delta x_{average}$.

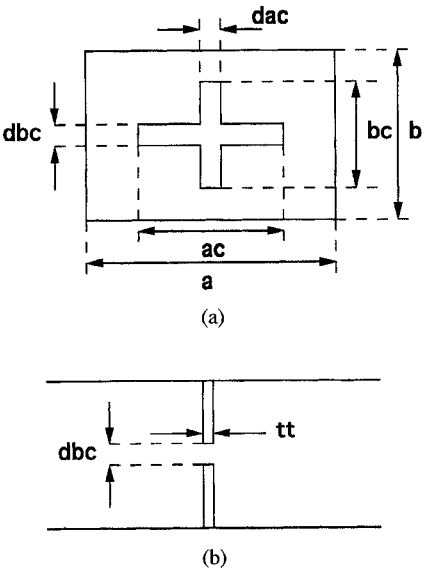

Fig. 12. Cross-shaped iris in rectangular waveguide: (a) y–z view and (b) x–y view.

the mesh nonuniformity. It is interesting to note that an exponentially varying grid gives a slope for the average error that is twice the slope of the uniform grid.

C. Error Analysis with the Perfectly Matched Layer

In this analysis, we use meshes that combine exponentially increasing cell sizes with abrupt changes. PML's are used to absorb the TE_{10} waves, a monochromatic source is used to excite the field, and the discrete Fourier transform is used at each nodal point. When implementing the PML, we use 40 layers of cells in the x-direction, $(\sigma_x, \sigma_x^*, 0, 0, 0, 0)$, giving a theoretical reflection coefficient of -100 dB, that in practice is reduced to about -80 dB. In Fig. 10 is plotted the maximum error versus maximum spatial increment, and the average error versus the average cell dimension. The least square fit to

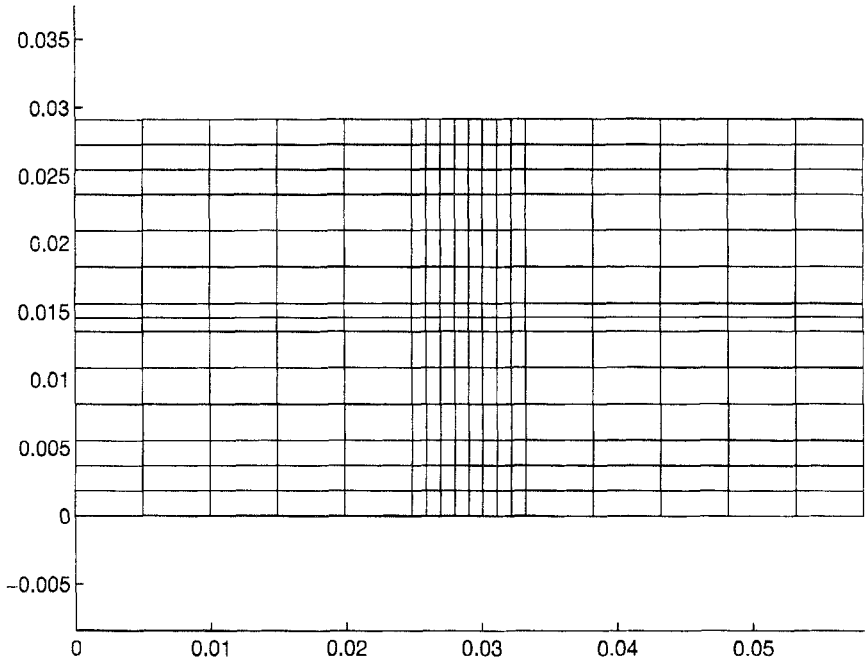

Fig. 13. Mesh for the cross-shaped iris in rectangular waveguide Dimensions in inch: $ac = 0.331$, $bc = 0.711$, $dbc = dac = 0.080$, $tt = 0.016$

the data in Fig. 10 gives a slope of 2.827 when considering maximum error versus maximum cell size, and a slope of 3.942 for the average error versus average cell size.

D. Error Analysis with Imperfectly Absorbing Boundary Conditions

In this case we apply the dispersive boundary condition to the waveguide problem, assuming that the two plane waves that propagate in the waveguide impinge on the boundary with normal incidence (Mur's first-order absorbing boundary [23]). This absorbing boundary condition is less than perfect and the application of an imperfect absorbing boundary condition gives a truncation error in the field calculation that is added to the error of the spatial discretization. The same mesh as was used in case (C) was used for the present analysis along with the same TE_{10} source. Results giving the maximum error versus maximum cell dimension, and the average of both are presented in Fig. 11. With use of the imperfectly absorbing boundary condition, the total error is found to degrade to first-order accuracy. Based on the results given in Section III, we conclude that this degradation is exclusively due to the truncation error in imperfectly boundary conditions.

IV. Application of the Nonuniform FDTD to Discontinuities in Waveguides

One of the more attractive application areas for nonuniform FDTD is in modeling waveguide discontinuities. In this section, we show the application of the nonuniform FDTD to the analysis of very narrow iris in rectangular waveguides. The waveguide dimensions we used were 2.29×1.145 inch^2, in other words 58.166×29.083 mm^2. A cross-shaped iris was used, as is shown in Fig. 12, having a width of 0.08 inch, (2.032 mm), which is 28 times narrower than the width of the waveguide. The use of an uniform mesh in this analysis would demand a 57×28 mesh be used in the cross section of the waveguide. This requirement for the mesh size is brought about by the need for a mesh is consistent with the dimensions of the cross-shaped iris. An alternative to the use of a dense mesh would be to use of the small hole formalism of [16]. Test results obtained using this approach showed appreciable errors in the time domain results. These errors (deviations) are likely to be amplified when a Fourier transform is used to move from the time domain to the frequency domain.

A Gaussian modulated pulse was used as the source of the excitation, the frequency bandwidth of the pulse is determined by the amplitude (shape) of the pulse, A, and the central frequency f_c is defined by the frequency of the modulated sinusoid. The transversal shape of the excitation corresponds to that of the TE_{10} mode, and the time domain dependence is,

$$e_i(t) = \sin(2\pi f_c t) \exp \frac{(t - t_0)^2}{A^2}. \tag{25}$$

Twenty PML's were used to simulate a perfectly matched waveguide model with a theoretical reflection coefficient of -80 dB. The PML is better suited to waveguide analysis than are other second-order absorbing boundaries because of its simplicity and its adaptivity. In the first instance, only layers that need to be adopted are those that absorb waves propagating in the x-direction i.e., $\sigma = (\sigma_x^*, \sigma_x, 0, 0, 0, 0)$. Secondly, the performance of the absorbing boundary condition can be altered by adding more layers or by changing the conductivity profile of the layers. The existing second-order dispersive absorbing boundaries [12], [19], only exactly absorb the propagating wave for two frequency components and are difficult to implement in a general nonuniform mesh.

A cross shaped iris with arm dimensions $ac = 0.331$ inch, and $bc = 0.711$ inch, and thicknesses $dbc = dac = 0.080$ inch, $tt = 0.016$ inch was analyzed first. We used

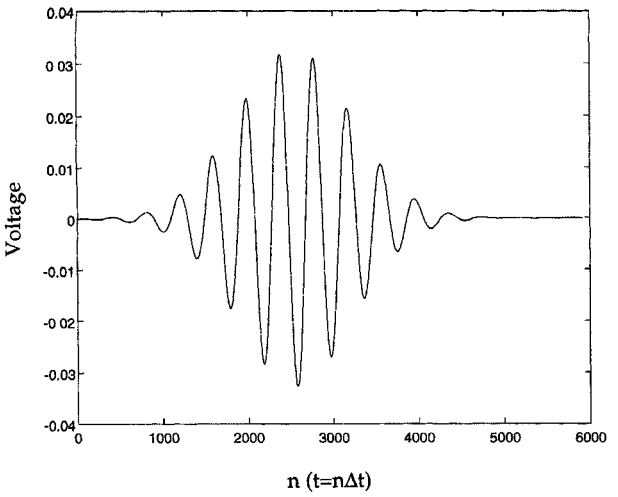

Fig. 14. Incident field pulse through the cross-shaped iris of Fig. 13.

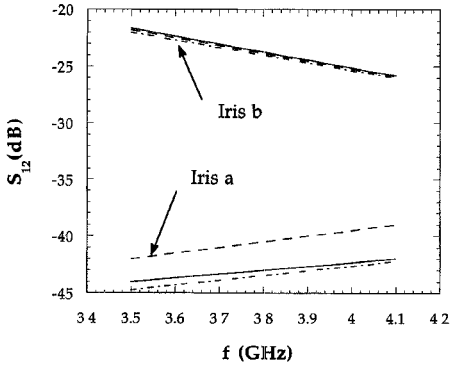

Fig. 15. Transmission coefficient for two cross-shaped-iris: (- - -) mode matching, (——) Measurements, (-.-.-) FDTD. IRIS a (Fig. 13): Dimensions (inch), ac = 0.331, bc = 0.711, dbc = dac = 0.080, tt = 0.016. IRIS b: Dimensions (inch), bc = 0.331, ac = 0.711, dbc = dac = 0.080, tt = 0.016.

a mesh with dimensions 120 × 14 × 18 in the x, y, and z–directions. The nonuniform mesh topology shown in Fig. 13, was used in the y–z plane. A uniform mesh with $\Delta x = tt$, was used in the x-direction. In Fig. 14, is shown the pulse that is incident upon the discontinuity having a frequency bandwidth from 3.5–4.1 GHz. The pulse that emerges from the other side of the discontinuity is almost negligible. The transmitted signal level is almost −50 dB down with respect to that of the incident signal. Fig. 15 gives a comparison of the transmission coefficients obtained using FDTD, mode matching, and measurements. Surprisingly the FDTD results are in better agreement with the measurements than those from mode matching. For f = 3.5 GHz the mode matching S_{12} is −42 dB, the experimental value was −44 dB, and the FDTD result was −44.7 dB, for f = 4.1 GHz, MM gave −39, experimental −42, and FDTD −42.2. In Fig. 15, is given a comparison of FDTD results for the same iris analyzed earlier, only this time with the iris rotated by 90°, with MM results and measurements.

V. Conclusion

An investigation was carried out on the viability of using the FDTD method with nonuniform meshes. In particular, we looked at the errors generated by using nonuniform meshes and found them to be of second-order with respect the cell sizes. This numerical analysis was based on the assumption that "exact" boundary conditions were used to terminate the far end of the waveguide. The PML technique is adapted for use with the nonuniform FDTD method and found to behave like an "exact" boundary condition. It was shown that the accuracy of the nonuniform FDTD method degrades to first-order if less than exact boundary conditions are used. The nonuniform FDTD method is shown to be highly useful for the analysis of waveguides and is particularly suited to the analysis of discontinuities in waveguides, such as a waveguide iris.

References

[1] K. S. Yee, "Numerical solution of initial boundary value problems involving Maxwell's equations in isotropic media," *IEEE Trans. Antennas Propagat.*, vol. AP-14, pp. 302–307, May 1966.

[2] A. Taflove and K. R. Umashankar, "Review of FD-TD numerical modeling of electromagnetic wave scattering and radar cross section," in *Proc. IEEE*, vol. 47, 1986, pp. 421–435.

[3] X. Zhang and K. K. Mei, "Time-domain finite difference approach to the calculation of the frequency-dependent characteristics of microstrip discontinuities," *IEEE Trans. Microwave Theory Tech.*, vol. 36, pp. 1775–1787, 1988.

[4] K. Li, C. F. Lee, S. Y. Poh, R. T. Shin, and J. A. Kong, "Application of FDTD method to analysis of electromagnetic radiation from VSLI heatsink configurations," *IEEE Trans. Electromagn. Compat.*, vol. EMC-35, no. 2, pp. 204–214, 1993.

[5] V. J. Brankovic, D. V. Krupezevic, and F. Arndt, "An efficient two-dimensional graded mesh finite-difference time-domain algorithm for shielded or open waveguide structures," *IEEE Trans. Microwave Theory Tech.*, vol. 40, pp. 2272–2277, 1992.

[6] D. L. Paul, N. M. Pothecary, and C. J. Railton, "Calculation of the dispersive characteristics of open dielectric structures by the finite-difference time-domain method," *IEEE Trans. Microwave Theory Tech.*, vol. 42, pp. 1207–1212, 1994.

[7] H. Sundqvist and G. Veronis, "A simple finite-difference grid with nonconstant intervals," *Tellus*, vol. 22, pp. 26–31, 1970.

[8] E. Kalnay de Rivas, "On the use of nonuniform grids in finite-difference equations," *J. Comput. Phys.*, vol. 10, pp. 202–210, 1972.

[9] T. A. Manteuffel and A. B. White, "The numerical solution of second-order boundary value problems on nonuniform meshes," *Math Comp.*, vol. 47, pp. 511–535, Oct. 1986.

[10] P. Monk and E. Suli, "A convergence analysis of Yee's scheme on nonuniform grids," *SIAM J. Numerical Anal.*, vol. 31, pp. 393–412, 1994.

[11] E. Suli, "Convergence of finite volume schemes for Poisson's equation on nonuniform meshes," *SIAM J. Numerical Anal.*, vol. 28, pp. 1419–1430, 1991.

[12] E. A. Navarro, L. Gallart, J. L. Cruz, B. Gimeno, and V. Such, "Accurate absorbing boundary conditions for the FDTD analysis of H-plane waveguide discontinuities," *IEE Proc. Microwave Antennas Propagat.*, vol. 141, pp. 59–61, 1994.

[13] J. Berenger, "A perfectly matched layer for the absorption of electromagnetic waves," *J. Computat. Phys.*, vol. 114, pp. 185–200, 1994.

[14] D. S. Katz, E. T. Thiele, and A. Taflove, "Validation and extension to three dimensions of the Berenger PML absorbing boundary condition for FD-TD meshes," *IEEE Microwave Guided Wave Lett.*, Aug. 1994.

[15] E. A. Navarro, C. Wu, P. Y. Chung, and J. Litva, "Application of PML superabsorbing boundary condition to nonorthogonal FDTD method," *Electron Lett.*, vol. 30, no. 20, pp. 1654–1656, 1994.

[16] B.-Z. Wang, "Small-hole formalism for the FDTD simulation of small-hole coupling," *IEEE Microwave Guided Wave Lett.*, vol. 5, pp. 15–17, Jan. 1995.

[17] J. A. Stratton, *Electromagnetic Theory*. New York: McGraw-Hill, 1941.

[18] J. G. Blaschak and G. A. Kriegsmann, "A comparative study of absorbing boundary conditions," *J. Comput. Phys.*, vol. 77, pp. 109–139, 1988.

[19] Z. Bi, K. L. Wu, C. Wu, and J. Litva, "A dispersive boundary condition for microstrip component analysis using FD-TD method," *IEEE Trans. Microwave Theory Tech.*, vol. MTT-40, pp. 774–777, 1992.

[20] R. Holland, "Finite-difference time-domain (FDTD) analysis of magnetic diffusion," *IEEE Trans. Electromagn. Compat.*, vol. EMC-36, pp. 32–39, 1994.

[21] E. A. Navarro, C. Wu, P. Y. Chung, and J. Litva, "Some considerations about the finite difference time domain method in general curvilinear coordinates," *IEEE Microwave Guide Wave Lett.*, vol. 4, no. 12, pp. 396–398, 1994.

[22] E. A. Navarro and V. Such, "Study of TE and TM modes in waveguides of arbitrary cross-section using a FD-TD formulation," *IEE Proc. Microwave Antennas Propagat.*, vol. 139, pp. 491–494, 1992.

[23] G. Mur, "Absorbing boundary conditions for the finite-difference approximation of the time domain electromagnetic field equations," *IEEE Trans. Electromagn. Compat.*, vol. EMC-23, pp. 377–382, 1981.

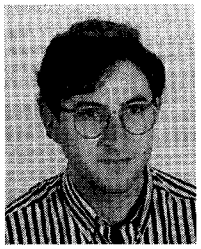

Enrique A. Navarro was born in Sueca (València), Spain, in 1965. He received the Licenciado degree in physics in 1988 and the Ph.D. degree in 1992, both from the Universitat de València, Spain.

From 1988 to 1989, he was working at Grupo de Mecánica del Vuelo S.A. (GMV S.A.), Madrid. He was a Fellow at the Universitat de València from 1989 to 1991, where he was teaching and doing research. Since 1991, he has been an Assistant Professor in the Department of Applied Physics at the Universitat de València. He was recipient of a NATO fellowship in 1993 and he was a Visiting Professor at the Communications Research Laboratory of McMaster University, Hamilton, Ontario, Canada in 1994. His current research interests include numerical methods in electromagnetics and intelligent antennas for PCS.

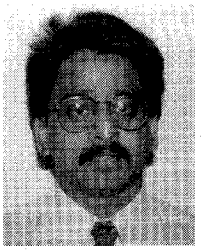

Nagula T. Sangary was born in Jaffna, Sri-Lanka in 1964. He received the B.Sc. in electrical engineering from Texas A&I University, in 1988, and M.Eng. in electrical engineering from McMaster University, Canada, in 1994.

In 1995, he joined Nortel Technology (Bell Northern Research) working on CDMA hardware, and concurrently he is working on the Ph.D. degree in electrical engineering at McMaster University. His research interests include design and analysis of microwave devices.

Mr. Sangary is a member of engineering honors societies Eta Kappa Nu and Tau Beta Pi.

John Litva (SM'92) is currently the Director of the Communications Research Laboratory (CRL), a Professor in Electrical and Computer Engineering at McMaster University, Hamilton, Ontario, Canada, and an Advisory Professor at the Nanjing University of Science and Technology in Nanjing, China. He is also the Director of the CRL, which is a separate research institute located at McMaster University. The CRL carries out research in the areas of signal processing, software engineering, microwaves, computer modeling and antennas. Research is directed toward applications in satellite and terrestrial communications, and in particular, PCS. He has published more than 100 papers and has lectured widely on selected topics in numerical techniques for analyzing microstrip antennas, digital beamforming, nonlinear and adaptative beamforming, integrated antennas, and simulation and analysis of multipath signals. At present, his research interests are digital beamforming for satellite communications, intelligent antennas for PCS, electromagnetic modeling, and propagation measurements, modeling, and simulations for PCS.

Dr. Litva is the holder of the Microwave Antenna Chair sponsored by Spar Aerospace and NSERC, as well as being a Thrust Leader in the Telecommunications Research Institute of Ontario (TRIO). TRIO is a university-industry based Center of Excellence, which is funded by the Province of Ontario, and whose mandate is to conduct research in support of the telecommunications industry in Ontario.